HAL
open science

Physical Model for Studying the Migration of Fine Particles in the Railway Substructure

Trong Vinh Duong, Yu-Jun Cui, Anh Minh A.M. Tang, Jean Claude Dupla, Jean Canou, Nicolas Calon, Alain Robinet, Baptist Chapot, Emmanuel de Laure

To cite this version:

Trong Vinh Duong, Yu-Jun Cui, Anh Minh A.M. Tang, Jean Claude Dupla, Jean Canou, et al.. Physical Model for Studying the Migration of Fine Particles in the Railway Substructure. Geotechnical Testing Journal, 2014, 37 (5), pp.895-906. 10.1520/GTJ20130145 . hal-01111314

HAL Id: hal-01111314

https://enpc.hal.science/hal-01111314v1

Submitted on 25 Apr 2018

HAL is a multi-disciplinary open access archive for the deposit and dissemination of scientific research documents, whether they are published or not. The documents may come from teaching and research institutions in France or abroad, or from public or private research centers.

L'archive ouverte pluridisciplinaire **HAL**, est destinée au dépôt et à la diffusion de documents scientifiques de niveau recherche, publiés ou non, émanant des établissements d'enseignement et de recherche français ou étrangers, des laboratoires publics ou privés.

A physical model for studying the migration of fine particles in railway sub-structure

Duong T.V.[1], Cui Y.J.[1], Tang A.M.[1], Dupla J.C.[1], Canou J.[1], Calon N.[2], Robinet A.[2], Chabot B.[1], De Laure E.[1]

[1]: Ecole des Ponts ParisTech, U.R. Navier/CERMES, 6 – 8 av. Blaise Pascal, Cité Descartes, Champs – sur – Marne, 77455 Marne – la – Vallée cedex 2, France

[2]: French Railway Company (SNCF)

Corresponding author:

Prof. Yu-Jun CUI

Ecole des Ponts ParisTech

6-8 av. Blaise Pascal, Cité Descartes, Champs-sur-Marne

F-77455 Marne – la – Vallée cedex - France

Telephone: +33 1 64 15 35 50

Fax: +33 1 64 15 35 62

E-mail : yujun.cui@enpc.fr

Abstract

In order to study the creation of interlayer and the mud pumping phenomena in the conventional French railway substructure, a physical model was developed with a 160 mm thickness ballast layer overlying a 220 mm thickness artificial silt layer (mixture of crushed sand and kaolin), both layers being compacted in a cylinder of 550 mm inner diameter. One positive pore water pressure sensor, three tensiometers and three TDR sensors were installed around the ballast/silt interface allowing the evolution of pore water pressure (negative or positive) and volumetric water content to be monitored, respectively. A digital camera was installed allowing direct monitoring of different movements (ballast, ballast/sub-soil interface, etc.). The effects of loading (monotonic and cyclic loadings) and degree of saturation of sub-soil (w = 16%, S_r = 55% and near saturation state) were investigated. It was found that the development of pore water pressure in the sub-soil is the key factor causing the migration of fine particles that results in the creation of interlayer as well as the mud pumping. In particular, thanks to the camera, the pumping up level of fine particles was visualized during the test, showing that the migration of fine particles was not only due to the interpenetration of ballast particles and sub-soil, but also the pore water pressure that pushed the fine particle upwards. The relevant results obtained proved that the experimental set-up is appropriate to be used in investigating the degradation of railway sub-structure.

Keywords: railway substructure; physical model; cyclic loading; pore water pressure; interlayer creation; mud pumping.

Introduction

Problems related to track settlement and stability come not only from the degradation of each layer but also from the interaction between layers. Very often, fine particles migration from sub-grade results in changes of sub-structure components, corresponding to mud pumping or creation of interlayer. Mud pumping is characterized by the migration of sub-soil fine particles in the ballast layer. It was widely recognized in both the railway context (Ayres 1986, Selig and Waters 1994, Raymond 1999, Voottipruex and Roongthanee 2003, Burns et al. 2006, Gataora et al. 2006, Aw 2004, 2007, Indraratna et al. 2011) and the pavement context (Yoder 1957, Van 1985, Alobaidi and Hoare 1994, 1996, 1998a, 1998b, 1999, Zhang 2004, Yuan et al. 2007). By contrast, the interlayer has been identified and characterized only recently (Calon et al. 2010, Trinh et al. 2011, Trinh 2011, Trinh et al. 2012, Cui et al. 2013, Duong et al. 2013). This interlayer mainly involves the conventional lines. Indeed, the conventional lines in France were constructed more than one hundred years ago by directly putting ballast onto the sub-grade (unlike the new lines for high speed trains). Over years of operation, the interlayer was formed mainly by the interpenetration between the sub-grade soil and ballast under the effect of train action. As both mud pumping and presence of interlayer can significantly affect the track mechanical behavior, it appears important to investigate the related mechanisms in-depth.

Up to now, even migration of fine particles and its consequence have been reported in several studies, the knowledge on the driving mechanisms is still limited. Indeed, in the case of interlayer, its creation is still an open question. For the mud pumping, some different mechanisms were proposed. Takatoshi (1997) reported that pumping of fine particles is due to the effect of suction generated by the upward and downward movement of ties. Differently, Alobaidi and Hoare (1996, 1999) proposed that pumping of fine particles depends mainly on the pore water pressure developed at the interface between the sub-grade and sub-base/ballast layer.

As far as the experimental work is concerned, few studies have been undertaken in the laboratory. Alobaidi and Hoare (1996) developed an apparatus from a modified 350 mm triaxial cell. Using this apparatus, the pumping of fine particles in highway pavement was investigated under 2 Hz loading on a 32 mm diameter metallic hemisphere representing the sub-base material. However, this prototype apparatus and the adopted methodology are not suitable for the railway issue (metallic hemisphere instead of ballast, low loading frequency), and in addition, the pumping level of fine particles was only recorded at the end of the test. Burns et al. (2006) and Ghataora et al. (2006) developed a 230 mm diameter steel cylinder to test a 200 mm thick sub-grade beneath a 75 mm thick ballast layer. In this case, the diameter of the cylinder seems to be small when considering the ballast size (about 60 mm). Moreover, the monitoring of the intermixing of sub-soil particles and ballast particle is also not allowed.

In this study, a physical model was developed, allowing the mud pumping and the creation of interlayer to be investigated. The model had a diameter of 550 mm that is considered as large enough to minimize any size effect. The apparatus was equipped with 3 tensiometers and 3 time domain reflectometer (TDR) allowing the monitoring of pore water pressure and volumetric water content at different positions, respectively. Moreover, a digital camera was used to monitor the evolution of the interface between ballast and sub-soil. In order to study the creation of interlayer within the sub-structure of conventional lines in the French railway network, the sample was prepared with a ballast layer overlying a sub-soil layer. This configuration represents the conventional railway sub-structure at the moment of construction (more than one hundred years ago). The mud pumping phenomenon was also investigated.

Materials

In order to have a quantity of homogeneous sub-soil large enough for conducting the experimental investigation planned, the sub-soil used in this study was produced artificially by mixing 30% Kaolin Speswhite clay and 70 % crushed sand C10 (by dry mass). It is named henceforth *70S30K*. The reason of

using this artificial material is that it can be reproduced easily in the laboratory for having a large quantity needed for the whole test program, thus avoiding any problems related to the natural soil heterogeneity – the composition of soil can be slightly different from one sample to another. Figure 1 shows the grain size distribution curves of Kaolin Speswhite clay, of the crushed sand C10 (given by suppliers) and of the mixture *70S30K* (determined using the dry sieving and the hydrometer methods). Note that the curve of *70S30K* is close to that of the Jossigny silt, a soil widely studied worldwide for its hydro-mechanical behavior especially in the unsaturated state (see Cui and Delage 1996 for instance). The Standard Proctor curve of *70S30K* is plotted in Figure 2; its hydraulic conductivity at a dry unit mass of 1.5 Mg/m^3 is 8.4×10^{-7} m/s. Some other properties are presented in Table 1.

The ballast used in this study was taken from the storage of construction materials of the French Railway company (SNCF). It is a granular material with d/D = 25/50 mm. The maximum diameter of ballast is 63 mm. Detailed characteristics of the conventional ballast can be found in SNCF (1995) and Al Shaer (2005).

Experimental setup and procedures

Figure 3 presents schematic views of the physical model including a 3D view (Figure 3a), a side view (Figure 3b) and a cross section (Figure 3c). The wall of the apparatus was made of Poly(methyl methacrylate) (PMMA) which is a transparent thermoplastic allowing an external observation by digital camera. The transparent cell has an internal diameter of 550 mm, a wall thickness of 20 mm and a height of 600 mm. With these dimensions, any size effect is expected to be minimized as the ratio of the apparatus diameter to that of ballast particles is larger than 10. Indeed, this ratio is two times the value recommended by the AFNOR standard (2004) and the values adopted by other authors (Yasuda et al. 1997, Lackenby et al. 2007, Ekblad 2008). The column has different holes that can host 10 tensiometers and 5 TDRs at different heights. These holes are divided into three groups disposed at 90°; groups 1 and

3 are for the tensiometers and group 2 is for TDRs. Note that during the test when a hole was not used for sensor installation, it was filled by a special plug having the same dimensions of the hole in order to not affect the test. In this study, only three volumetric water content sensors (TDR1 to TDR3) and three tensiometers (T1 to T3) were installed along the column at different heights: h = 120, 160 and 200 mm (the elevation is measured from the bottom of the apparatus). These positions were chosen in order to have maximum information about the pore water pressure and volumetric water content not only at the position (200 mm) near the interface between the sub-soil and the ballast but also inside the sub-soil layer (120 mm). On the top of the PMMA wall, a Light-Emitting Diode (LED) series was installed lighting up the apparatus wall and thus improving the observation quality by the digital camera. The PMMA cylindrical wall was fixed on a metallic base plate using screws. A porous plate and a geotextile were placed at the bottom of the sample to ensure uniform water distribution and to avoid any loss of soil particles. At the bottom of apparatus (h = 0 mm), a pressure transducer was installed for measuring the positive pore water pressure in saturated case.

For the specimen preparation, crushed sand (C10) and clay (kaolin Speswhite) were mixed up with water to obtain the target water content - the optimum water content w = 16 % (see Figure 2). After mixing, the wet material was stored in hermetic containers for at least 24 h for moisture homogenization. The soil specimen was prepared by manual compaction in five layers of 40 mm thick each and one layer of 20 mm thick, making a total of 220 mm thickness for the whole specimen. In the literature involving the study on the migration of fine particles, the value of dry unit mass considered is often around 1.50 Mg/m^3: 1.45 Mg/m^3 in Burns et al. (2006) and from 1.52 to 1.54 Mg/m^3 in Alobaidi et al (1999). According to Burns et al. (2006), this value corresponds to the medium strength in field conditions. Thereby, the dry unit mass of 1.50 Mg/m^3 was chosen in this study. With the specific gravity of clay and crushed sand (see Table 1), the corresponding porosity and the degree of saturation calculated are 43% and 55%, respectively. The TDR probes were installed during the specimen compaction between the

sub-layers of sub-soil at the target heights. Once the sub-soil was compacted, 160 mm ballast was placed on the sub-soil and the ballast particles were arranged in order to have a satisfactory horizontal surface between ballast and piston. After the specimen preparation, the whole column was placed under the hydraulic actuator. The tensiometers were then installed, and other operations were undertaken such as lighting up the LED series, setting up the digital camera, preparing the loading program. Figure 4 presents a photograph of the column with specimen.

The test was carried out in three stages. In the first stage (namely henceforth *Unsaturated state*) where the sub-soil was in unsaturated state (w = 16 %; S_r = 55%), a pre-loading (including monotonic loading and cyclic loading at low frequency) was firstly applied. Monotonic loading started from 0 to 100 kPa at a rate of 0.14 kPa/s. Afterwards, low frequency cyclic loading was applied with the axial stress varying from 30 to 100 kPa: 20 cycles at 0.1 Hz; 50 cycles at 1Hz and 100 cycles at 2 Hz. This pre-loading was applied in order to ensure the good functioning of the apparatus before applying a frequency as high as 5 Hz. The results during this stage are shown in Figure 5. A 5 Hz loading was applied afterwards for 500 000 cycles. Note that the choice of load amplitude and the frequency was made based on the consideration of loading conditions in the conventional sub-structure in France (see Trinh et al. 2012; Duong et al. 2013).

Basically, mud pumping is more pronounced when the sub-soil is saturated. For this reason, after the first stage – *Unsaturated sate*, a second stage namely Saturation followed by a third stage namely *Saturated state* was applied. During the saturation, the sub-soil was saturated from the bottom under a hydraulic head of 12 kPa using an external water source connected to the column. The water level was maintained at 2 cm above the ballast/sub-soil interface in order to ensure the fully saturated state of the sub-soil layer. Meanwhile, a sensor of pore water pressure was installed at h = 0 mm. In *Saturated state*, monotonic loading at the same increase rate as in *Unsaturated state* was applied up to 100 kPa followed

by the 5 Hz cyclic loading. The test ended when fine particles were observed at the surface of ballast layer.

During the test, the variation of pore water pressure was recorded with 3 home-made tensiometers that are based on the same principle as the high capacity tensiometers developed by Mantho (2005), Cui et al. (2008), Lourenço et al. (2011) and Toll et al. (2012). The working pressure range of these tensiometers is from 700 kPa to -700 kPa (they measure both positive pressure and suction). The time-domain reflectometry (TDR) was connected to a data logger - Trase BE allowing the dielectric constant K_a to be recorded, which is deduced from the crossing time of electromagnetic wave within the surrounding material. The accuracy of the measurement is ± 2%. The well-known model of Topp et al. (1980) was applied to calculate the volumetric water content:

$$\theta = -5.3\times10^{-2} + 2.92\times10^{-2} K_a - 5.5\times10^{-4} K_a^2 + 4.3\times10^{-6} K_a^3 \qquad (1)$$

Experimental results and discussions

Figure 5 presents the results obtained during the pre-loading in *Unsaturated state*. The variation of stress applied was plotted in Figure 5a where the stress was increased monotonically from 0 to 100 kPa and then cyclically at low frequency before the 5 Hz loading for 500 000 cycles at the end. It can be observed that during the monotonic loading, the axial displacement increased quickly and it continued to increase during the cyclic loading, to reach 7.3 mm. The displacement was decreased to 6.8 mm when the load decreased from 100 kPa to 30 kPa.

Figure 6 shows the evolution of global displacement in *Unsaturated state* (w = 16%). The displacement increased quickly during the monotonic loading, from 0 to 7.3 mm. The pre-cyclic loading at 0.1 Hz, 1 Hz and 2 Hz increased the permanent displacement to 8.7 mm. The increasing rate of permanent displacement was also high in the first period of 5 Hz loading (from 8.7 mm to 9.9 mm for

the first 10 000 cycles) and then it slowed down (it needs nearly 50 000 cycles to increase from 9.9 mm to 10.9 mm).

Figure 7 depicts the evolution of permanent displacement during the 5 Hz loading. It shows that the displacement tended to increase linearly with the logarithm of cycle number N when $N > 100$. This is in agreement with the results of some previous studies. Indeed, in Paute and Le Fort (1984), Hornych (1993) and AFNOR (1995) for the unbound granular materials, the permanent displacement value at 100 cycles was considered as the reference value in the modeling of ballast axial displacement after 100 cycles. In these models, the displacement evolution varies also linearly with the loading cycle number $\log N$.

From the image by the digital camera (Figure 8a), the movement of one ballast particle was monitored. The movement during *Unsaturated state* of this ballast particle was analyzed by considering the change in its contour (Figure 8b). It can be observed that there is not only vertical displacement but also horizontal one, indicating a rotation of the ballast particle. In general, the movements of other ballast particles follow the same trend. This suggests that ballast particles rearranged between themselves during the cyclic loading.

Figure 9 presents the evolution of volumetric water content (Figure 9a) and pore water pressure (Figure 9b) during the *Unsaturated state*. The initial volumetric water contents are θ = 21.6 %, 22.7% and 17.9% at h = 120 mm, 160 mm and 200 mm, respectively. Note that the 200 mm level corresponds to 20 mm below the ballast/sub-soil interface. As it was the last layer for the compaction operation, its dry unit mass can be smaller than those of lower layers.

As the sub-soil layer was fully saturated, the variation of volumetric water content θ can be used to estimate its settlement by assuming that soil particles and water are not compressible.

The total height is divided into three sub-layers, assuming constant volumetric water content in each sub-layer. The calculation of the settlement of each sub-layer is as follows:

$$\Delta V_{total} = h_1 \times A - \frac{Vwater}{\theta_2}$$

$$\Delta h \times A = h_1 \times A - \frac{(h_1 \times A) \times \theta_1}{\theta_2} \qquad (2)$$

$$\Delta h = h_1 \times \left(1 - \frac{\theta_1}{\theta_2}\right)$$

where ΔV_{total} and Δh are the variations of total volume and settlement of the sub-layer, respectively; θ_1 and θ_2 are respectively the volumetric water contents before and after the loading; V_{water} is the volume of water in the sub-layer, A is the cross section of the specimen, h_1 is the thickness of sub- layer before loading.

The final settlement is the summary of the settlements of all sub-layers:

$$\Delta h = \Delta h_{120} + \Delta h_{160} + \Delta h_{200} \qquad (3)$$

The settlement result obtained is also presented in Figure 6. It can be observed that the calculated settlement has the same trend as the displacement by external measurement but slightly larger. Note that the external displacement consists of both the displacements of ballast layer and sub-soil layer while the calculated settlement consists of only the part of sub-soil. Note also that the accuracy of TDR used is 2% that corresponds to a settlement of 4.3 mm.

During the 5 Hz loading for 500 000 cycles, the volumetric water content was almost stable with small variations (Figure 9a). From the beginning to the end of the 5 Hz loading, the values are 22.2 ± 0.2% for TDR1 at h = 120 mm, 23.4 ± 0.3% for TDR2 at h = 160 mm and 20.9 ± 0.5% for TDR3 at h =

200 mm. On the whole, the degree of saturation of the whole sub-soil layer varied from 49% to 54%; this is quite close to the theoretical value of S_r, estimated at 55 %.

The response of tensiometers was plotted in Figure 9b. The curves of T1 (h = 120) and T2 (h = 160) are very close while the curve of T3 (h = 200) is clearly above. However, the shapes of the three curves are the same. After 20 h, the pore water pressure at all three levels reached their stabilization values: -166.4 kPa at h = 120 mm; -163.9 kPa at h = 160 mm and -114.1 kPa at h = 200 mm.

For the visual monitoring, two photographs were taken, one before the monotonic loading and another after the 5Hz loading for 500 000 cycles, and they are presented in Figure 10a and Figure 10b, respectively. Referring to the level of the top surface of the sub-soil layer, these two photographs show that the level of ballast/sub-soil interface did not change. Furthermore, no migration of fine particles was observed. This suggests that the sub-soil displacement calculated from θ does not represent the global variation. Note that the local ballast/sub-soil contact was not uniform over the whole interface section because ballast particles are very angular and have different shapes. This non-uniform contact can lead to non-uniform stress, thus a larger compression in the zones just beneath ballast particles as compared to the zones among particles. The TDR whose size is 80 mm long and 25 mm large was probably situated beneath ballast particles, giving rise to a higher θ value, hence a larger estimated settlement.

When the 5 Hz loading for 500 000 cycles ended, the sample was connected to an external water source and water was observed on the ballast/sub-soil interface after about 1 day. During this time, the volumetric water content measured by TDR increased consistently: the value at h =120 mm changed firstly, then it was the turn of h = 160 and finally of h = 200 mm (Figure 11a). At t = 45 h, the volumetric water contents at three levels stabilized. If one assumes that the dry unit mass of the sub-soil did not change during the test, the degree of saturation S_r was 87% to 88%. This is possible because during the saturation of very fine soil, it takes longtime to filling micro-pores. This can be observed also in Figure

11b where the evolution of pore water pressure is depicted. Till t = 45 h, the pore water pressure increased as the volumetric water content increased. Afterwards, although the volumetric water content θ became stable, the pore water pressure continued to increase up to zero. Furthermore, the three pore water pressure-time curves show the same increase trend (Figure 11b), suggesting that the process of filling micro-pores took place continuously and uniformly within the sample.

Once all the tensiometers gave the positive pressure values, the third stage (*Saturated state*) started with the monotonic loading followed by the 5 Hz cyclic loading. Figure 12 shows the variations of the pressure applied (Figure 12a), the permanent axial displacement (Figure 12b), the pore water pressure (Figure 12c) and the volumetric water content (Figure 12d). When the monotonic load increased from 0 to 100 kPa, the permanent axial displacement increased from 9 mm to 28.6 mm, and the pore water pressure increased also: at h = 120 mm and h = 200 mm it increased quickly and reached around 30 kPa while at h = 0 mm and h = 160 mm it increases more gently. The gentle increase at h = 0 mm can be explained by the far distance of this position from the loading source and the low hydraulic conductivity of the soil, while the gentle increase at h = 160 mm can be explained by some technical problem of the sensor at this level as revealed by the verification after the test. When the monotonic loading finished, the pore water pressure at all the three levels decreased but remained higher than zero. This can be explained by the very low hydraulic conductivity of the sub-soil that did not allow quick water pressure dissipation.

Under the 5 Hz loading, the permanent displacement continued to increase rapidly. The pore water pressure became quickly higher than 40 kPa (except the late response at h = 160 mm, possibly due to the corresponding sensor performance). In the end, the value obtained was between 40 and 58 kPa. Note that the applied pressure varied from 30 kPa to 100 kPa. This suggests that the effective stress (total pressure minus pore pressure) became sometimes negative during the unloading (applied stress smaller than pore water pressure) and liquefaction occurred within the sub-soil. Note that the negative

value of effective stress has no-physical meaning; it implies simply that during unloading there were no longer contact between soil particles. Further study is needed to verify this point.

On one hand, the sharp increase of pore water pressure weakens the sub-soil and on the other hand its dissipation brings fine particles upward. This is the key factor for the migration of fine particles. This is also consistent with the observation reported by Aw (2007) and Indraratna et al. (2011): mud pumping was identified in the zone with presence of water which softens the base layer and allows the migration of the fine particles into the void spaces between ballast particles, and also the penetration of ballast particles into the sub-grade under loading. The penetration of ballast and the migration of fine particles created a layer of mixture materials. This is probably the main mechanisms for the creation of interlayer identified in some railway sub-structures in France as mentioned before. In Figure 12d, the change of volumetric water content is insignificant: ± 1.4% at h = 120 mm, ± 1.9% at h = 160 mm and ± 2.4% at h = 200 mm. Their variation trends are different: the volumetric water content at h = 120 mm and 160 mm increased, while the value at h = 200 mm decreased continuously. These trends can be explained as follows: assuming that the sub-soil is nearly saturated, when the soil was compressed, the pore volume decreased. As a result, the volumetric water content increased at h = 120 mm and 160 mm. At h = 200, it is not very obvious because it was just 20 mm below the ballast/sub-soil interface that underwent significant modifications.

Figure 13 shows the photographs taken just before the monotonic loading (Figure 13a), after the monotonic loading (Figure 13b) and after the cyclic loading (Figure 13c) in *Saturated state*. The movement of fine particles can be identified. The fine particles were pumped up to the surface of ballast layer. During the monotonic loading, fine particles were also moving upwards, but not as rapidly as during the cyclic loading.

It can be seen that the fine particles migrated up to the ballast layer during the test (Figure 13). For a further analysis, the evolution of the sub-soil surface from the initial surface (after compaction) was recorded. From the images taken by camera (see Figure 13), the evolution of sub-soil surface was monitored by digitization and the results are presented in Figure 14. The intersection between the initial surface of sub-soil and the vertical ruler was chosen as the point zero in Figure 14. Each line represents the level of sub-soil surface at one moment of the test. The time interval between lines is 2 minutes. The first part (lower lines) corresponds to the variation during the monotonic loading and the second part (higher lines) corresponds to the variation during the cyclic loading (5 Hz). In general, the entire sub-soil surface was rising up. It is worth noting that when removing the sample at the end of the test, it was observed that the pumping up level of fine particles was uniform over the whole cross section.

In order to verify the nature of fines migration, let's take an assumption that this was the ballast penetration into the sub-soil that pushed the fine particle upward. In this way, a comparison between the volume of ballast particles in sub-soil and the volume of ballast layer voids filled by fine particles up-pumped was conducted. The volume occupied by ballast particles in sub-soil $V_{ballast}$ is calculated as follows:

$$V_{ballast} = \frac{h_{ballast} \times A}{1+e} \tag{4}$$

where $h_{ballast}$ is the settlement of ballast layer, A is the sample cross section and e is the void ratio of ballast layer.

The volume of ballast layer voids filled by fine particles of sub-soil V_{fines} can be calculated as follows:

$$V_{fines} = \frac{h_{fines} \times A}{1+e} e \tag{5}$$

where h_{fines} is the pumping up level of fine particles in the ballast layer. Admitting that ballast particles settlement pushed the fine sub-soil particles up and these fine particles fill the voids of ballast layer, i.e., $V_{ballast} = V_{fines}$. This leads to:

$$h_{fines} = \frac{h_{ballast}}{e} \tag{6}$$

Indraratna et al. (1997) proposed that the voids ratio of ballast *e* can vary from 0.74 (compacted) to 0.95 (un-compacted). In the case of the present study, as the sample was submitted to the 5 Hz loading for 500 000 cycles, the ballast layer can be considered as compacted with a void ratio equal to 0.74. As the ballast settlement under loading in *Saturated state* is 47.7 mm as presented in Figure 12b (the ballast settlement is considered equal to the piston displacement, the most critical case), the pumping up level estimated using Eq. (6) is 64.4. This value is much less than the real pumping up level of fine particles given in Figure 14: 113.1±15 mm. This suggests that there was not only the penetration of ballast particles pushing fine particles upwards, but also the dissipation of pore water pressure bringing fine particles up into the ballast layer, i.e. mud pumping occurred.

In order to have a better observation on the pumping up level of fine particles in the ballast layer, six reference vertical sections in Figure 14 (at the distances of 30 mm, 50 mm, 70 mm, 90 mm, 110 mm and 130 mm) were chosen. The evolutions of the sub-soil surface (pumping up levels) over time are determined and shown in Figure 15. This figure presents also the comparison between the real values of the sub-soil surface evolution with the theoretical value (Eq. 6). On the whole, the evolutions of the sub-soil surface at these sections follow the same trend. The interface rose up immediately when loading started. From Eq. (6), the theoretical pumping level of fine particles was calculated and the result is also presented in Figure 15. The calculated value is clearly lower than the real pumping level deduced from

the photographs. This confirms that the fine particles migration was not only due to the ballast penetration but also the dissipation of excess pore water pressure.

Conclusions

A physical model was developed to study the creation of interlayer and the mud-pumping phenomena in conventional railway sub-structure. The soil sample consisted of a ballast layer and one sub-soil layer. One pore water pressure sensor, three tensiometers, three TDRs were used to monitor the variations of pore water pressure and volumetric water content. The transparent PMMA apparatus wall and a digital camera allowed direct monitoring of the different movements (ballast, ballast/sub-soil interface, etc.). A test was carried out under monotonic and cyclic loading on a sample with the sub-soil in two different states: unsaturated and saturated sates. The results obtained allowed the migration of fine particles to be investigated. The following conclusions can be drawn:

1) The quality of the recorded data showed that the physical model developed worked well and the test protocol adopted was appropriate. Moreover, it was observed that the migration of fine particles was globally the same in every points of the interface, suggesting that the soil sample was representative of the one dimensional case. Thereby, the experimental set-up developed and the test procedure adopted are relevant for studying the mud pumping phenomenon occurring in the railway substructure.

2) In the unsaturated state of sub-soil, the interface between two layers did not change even after the 5 Hz loading for 500 000 cycles. On the contrary, in the near saturated state, it rose up very fast during the very first cycles. The difference between the two cases highlights the effect of water content which softens the base layer and allows the migration of the fine particles into the void spaces between ballast particles and also the penetration of ballast particles into the sub-grade.

3) The phenomenon produced in this test corresponds to the mud pumping phenomenon. The particle migration represents the intermixing between ballast and fine particles on one hand, and the fouling of railroad ballast by the underlying sub-soil on the other hand. The uniform pumping up level of fine particles confirms that the studied problem is one dimensional.

4) The mechanism behind the mud pumping phenomenon is the pore water pressure generation. Under cyclic loading, the pore water pressure can become higher than the total stress, giving rise to zero even negative effective stress. This is especially the case for the unloading phase. In this case, liquefaction occurs, that corresponds to the ideal condition for bring fine particles up under the effect of pore pressure dissipation. On the other hand, this is also the ideal condition for the penetration of ballast particles into the sub-soil, thus, for the interlayer creation. Note that the negative effective stress has no physical meaning; it implies simply that there were no longer any contact between soil particles and the unloading applied corresponded to a depression (suction) to water only. Further study is needed to verify this point.

Acknowledgements

This study was carried out within the research project “Reuse and reinforcement of conventional railway sub-structure and existing foundations”. The authors would like to address their deep thanks to Ecole des Ponts ParisTech (ENPC), Railway Network of France (RFF), French Railways Company (SNCF) and French National Research Agency for their supports.

References

AFNOR, 1995, “Essais Relatif aux Chaussées. Matériaux Non Traitées. Part 1 : Essai Triaxial à Chargements Répétés, NF P98-235-1”, French Standard (In French).

AFNOR, 2004, “Unbound and hydraulically bound mixtures. Part 7: cyclic load triaxial test for unbound mixtures,” *French standard*, NF EN 13286-7.

Al Shaer, A., 2005, “Analyse des Déformations Permanentes des Voies Ferrées Ballastées – Approche Dynamique”, PhD Dissertation, Ecole Nationale des Ponts et Chaussées, France (In French).

Alobaidi, I. and Hoare, D.J., 1994, “Factors Affecting the Pumping of Fines at the Subgrade- Subbase Interface of Highway Pavements: A Laboratory Study”, *Geosynthetics International*, Vol. 1, No. 2, pp. 221–259.

Alobaidi, I. and Hoare, D.J., 1996, “The Development of Pore Water Pressure at the Subgrade-Subbase Interface of a Highway Pavement and its Effect on Pumping of Fines”, *Geotextiles and Geomembranes*, Vol. 14, No. 2, pp. 111–135.

Alobaidi, I. and Hoare, D.J., 1998a, “Qualitative Criteria for Anti-pumping Geocomposites”, *Geotextiles and Geomembranes*, Vol. 16, No. 4, pp.221–245.

Alobaidi, I. and Hoare, D.J., 1998b, “The Role of Geotextile Reinforcement in the Control of Pumping at the Subgrade-Subbase Interface of Highway Pavements”, *Geosynthetics International*, Vol. 5, No. 6, pp. 619–636.

Alobaidi, I. and Hoare, D.J., 1999, “Mechanisms of Pumping at the Subgrade-Subbase Interface of Highway Pavements”, *Geosynthetics International*, Vol. 6, No. 4, pp. 241–259.

Aw, E.S., 2004, “Novel Monitoring System to Diagnose Rail Track Foundation Problems”, Master of Science Thesis, Massachusetts Institute of Technology, USA.

Aw, E.S., 2007, “Low Cost Monitoring System to Diagnose Problematic Rail Bed: Case Study at Mud Pumping Site”, Ph.D. Dissertation, Massachusetts Institute of Technology, USA.

Ayres, D.J., 1986, “Geotextiles or Geomembranes in Track? British Railway Experience”, *Geotextiles and Geomembranes*, Vol. 3, No. 2-3, pp. 129–142.

Burns, B., Ghataora, G.S. and Sharley, P., 2006, “Development and Testing of Geosand Composite Layers Using Pumps Index Test”, *In: Proceedings of the First International Conference on Railway Foundations Railfound06*, University of Birmingham, UK, pp. 355–366, ISBN10: 0-704426-00-5, ISBN13: 97807-04426-009.

Calon, N., Trinh, V.N., Tang, A.M., Cui, Y.J., Dupla, J.C., Canou, J., Lambert, L., Robinet, A. and Schoen O., 2010, “Caratérisation Hydraumécanique des Matériaux Constittutifs de Plateformes Ferroviaires Anciennes”. *Conférence JNGG2010*, Grenoble, France, p. 787–794 (In French).

Cui, Y. J. and Delage, P., 1996, “Yielding Behavior of an Unsaturated Compacted Silt”, *Géotechnique* Vol. 46, No. 2, pp. 291-311.

Cui, Y. J., Tang, A. M., Loiseau, C., and Delage, P., 2008, “Determining the Unsaturated Hydraulic Conductivity of a Compacted Sand-Bentonite Mixture Under Constant-Volume and Free-Swell Conditions”, *Physics and Chemistry of the Earth*, Parts A/B/C, Vol. 33, pp. S462–S471.

Cui, Y.J., Duong, T.V., Tang, A.M., Dupla, J.C., Calon, N. and Robinet, A., 2013, “Investigation of the Hydro-Mechanical Behaviour of Fouled Ballast”, *Journal of Zhejiang University- Science A*, Vol. 14, No.4, pp.244-255.

Duong, T.V., Trinh, V.N., Cui, Y.J., Tang, A.M. and Nicolas, C., 2013, “Development of a Large-Scale Infiltration Column for Studying the Hydraulic Conductivity of Unsaturated Fouled Ballast”, *Geotechnical Testing Journal*, Vol. 36, No. 1, pp. 54-63.

Ekblad, J., 2008, “Statistical evaluation of resilient models characterizing coarse granular materials,” *Materials and Structures*, Vol. 41, No. 3, pp. 509–525.

Ghataora, G.S., Burns, B., Burrow, M.P.N. and Evdorides, H.T., 2006, “Development of an Index Test for Assessing Anti-pumping Materials in Railway Track Foundations”, *In: Proceedings of the First International Conference on Railway Foundations*, *Railfound06*, University of Birmingham, UK, pp. 355–366.

Hornych, P., Corté, J.F. and Paute, J.L., 1993, “Etude des Déformations Permanents sous Chargements Répétés de Trois Graves non Traitées”, *Bulletin de Liaison des Laboratoires des Ponts et Chaussees*, Vol.184, pp. 77-84 (In French).

Paute, J.L. and Le Fort, R., 1984, “Determination of Untreated Gravels Mechanical Characteristics with Cyclic Loading Triaxial Apparatus”, *Bullein of the International Association of Engineering Geology*, No. 29, pp. 419 – 424, (In French).

Indraratna, B., Ionescu, D., Christie, D., and Chowdhurry, R., 1997, “Compression and Degradation of Railway Ballast under One-dimensional Loading”, *Australian Geomechanics Journal*, Vol 12, pp. 48 – 61.

Indraratna, B., Salim, W. and Rujikiatkamjorn. C., 2011, *Advanced Rail Geotechnology - Ballasted Track*. CRC Press.

Lackenby, J., Indraratna, B., Mcdowell, G., and Christie, D., 2007, “Effect of confining pressure on ballast degradation and deformation under cyclic triaxial loading,” *Géotechnique*, Vol. 57, No. 6, pp. 527 – 536.

Lourenço, S.D.N., Gallipoli, D., Toll, D.G., Augarde, C.E. and Evans, F.D., 2011, "A New Procedure for the Determination of Soil-water Retention Curves by Continuous Drying Using High-suction Tensiometers", *Canadian Geotechnical Journal*, Vol. 48, No. 2, pp. 327–335.

Mantho, A.T., 2005, "Echanges Sol-Atmosphère Application à la Sécheresse" Ph.D. Dissertation, Ecole Nationales des Ponts et Chaussées - Université Paris – Est, France (In French).

Raymond, G.P., "Railway Rehabilitation Geotextiles", *Geotextiles and Geomembranes*, Vol. 17, No. 4, pp. 213–230.

Selig, E.T. and Waters, J.M., 1994, *Track Geotechnology and Substructure Management*. Thomas Telford.

SNCF, 1995, "Specification Technique pour la Fourniture des Granulats Utilisés pour la Réalisation et l'Entretien des Voies Ferrées ST 590B", Technical guide (In French).

Takatoshi, I., 1997, "Measure for the stabilization of railway earth structure", *Japan Railway Technical Service.*

Toll, D.G., Lourenço, S.D.N. and Mendes, J., 2012, "Advances in Suction Measurements Using High Suction Tensiometers", *Engineering Geology*, doi:10.1016/j.enggeo.2012.04.013.

Topp, G.C., Davis, J.L. and Annan, A.P., 1980, "Electromagnetic Determination of Soil Water Content: Measurements in Coaxial Transmission Lines", *Water Resources Research*, Vol. 16, No. 3, pp. 574–582.

Trinh, V.N., 2011, "Comportement Hydromécanique des Matériaux Constittutifs de Plateformes Ferroviaires Anciennes". Ph.D. Dissertation, Ecole Nationales des Ponts et Chaussées - Université Paris – Est, France (In French).

Trinh, V.N., Tang, A.M., Cui, Y.J., Canou, J., Dupla, J.C., Calon, N., Lambert, L., Robinet, A. and Schoen, O., 2011, "Caractérisation des Matériaux Constitutifs de Plate-forme Ferroviaire Ancienne", *Revue Française de Géotechnique*, Vol. 134-135, pp. 65–74 (In French).

Trinh, V.N., Tang, A.M., Cui, Y.J., Dupla, J.C., Canou, J., Calon, N., Lambert, L., Robinet, A. and Schoen, O., 2012, "Mechanical Characterisation of the Fouled Ballast in Ancient Railway Track Sub-structure by Large-scale Triaxial Tests", *Soils and Foundations*, Vol. 52, No. 3, pp. 511-523.

Van, W. A., 1985, "Rigid Pavement Pumping: (1) Subbase Erosion and (2) Economic Modeling : Informational Report", *Publication FHWA/IN/JHRP-85/10. Joint Highway Research Project*, Indiana Department of Transportation and Purdue University, West Lafayette, Indiana, USA, doi:10.5703/1288284314094

Yasuda, N., Matsumoto, N., Yoshioka, R., and Takahashi, M., 1997, "Undrained monotonic and cyclic strength of compacted rockfill material from triaxial and torsional simple shear tests," *Canadian Geotechnical Journal*, Vol. 34, No. 3, pp. 357-367.

Yoder, E.J., 1957, "Pumping of Highway and Airfield Pavements: Technical Paper", *Publication FHWA/IN/JHRP-57/05. Joint Highway Research Project*, Indiana Department of Transportation and Purdue University, West Lafayette, Indiana, doi: 10.5703/1288284313518.

Yuan, R., Yang, Y.S., Qiu, X. and Ma, F.S., 2007, "Environmental Hazard Analysis and Effective Remediation of Highway Seepage", *Journal of Hazardous Materials*, Vol. 142, No. 1-2, pp. 381–388.

Zhang, C., 2004, "The Effect of High Groundwater Level on Pavement Sub-grade Performance", Ph.D. Dissertation, the Florida State University - College of Engineering, USA.

List of Tables

Table 1: Characteristic of sub-soil *70S30K*

List of Figures

Figure 1: Grain size distribution curve of studied material
Figure 2: Normal proctor curve of the sub-soil
Figure 3: Schematic view of the apparatus
Figure 4: Photograph of the physical model
Figure 5: Pre-loading in *Unsaturated state*
Figure 6: Axial displacement during loading in *Unsaturated state*
Figure 7: Displacement during cyclic loading at 5 Hz in *Unsaturated state*
Figure 8: Monitoring of one ballast particle movement
Figure 9: Changes in volumetric water content and pore water pressure in *Unsaturated state*
Figure 10: Photographs of the interface between two soils layers: a) before and b) after loading in *Unsaturated state*
Figure 11: Changes in volumetric water content and pore water pressure during *Saturation*
Figure 12: Test on the sub-soil at *Saturated state*: a) applied pressure; b) permanent axial displacement; c) pore water pressure and d) volumetric water content
Figure 13: Photographs showing the evolution of interface between two the soils layers: fine particles were pumped upwards
Figure 14: Sub-grade surface evolution
Figure 15: Pumping level of fine particles during the test in *Saturated state*

Table 1: Properties of sub-soil 70S30K

Specific gravity of clay G_s	2.6
Specific gravity of crushed sand G_s	2.65
Initial dry unit mass ρ_d	1.5 Mg/m^3
Porosity n	43%
Liquid Limit LL	27%
Plasticity Index IP	11%
Hydraulic conductivity K (ρ_d = 1.5 Mg/m^3)	8.4×10^{-7} m/s
Optimum water content w	16%

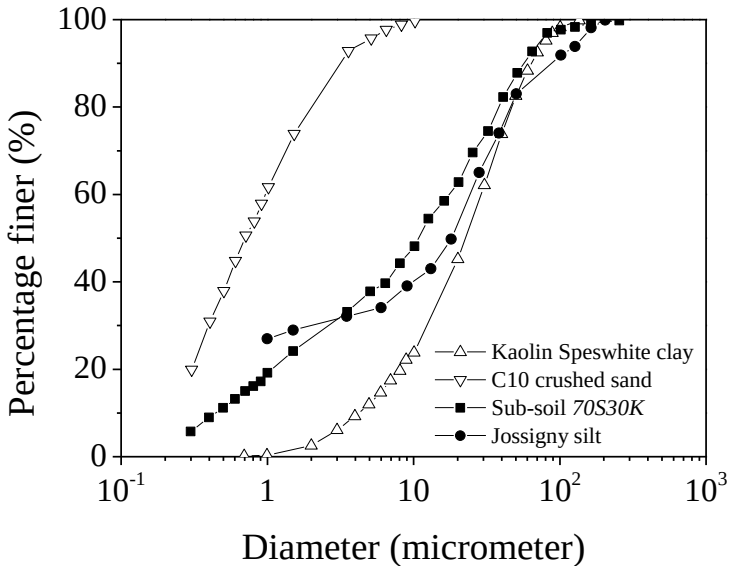

Figure 1: Grain size distribution curve of studied material

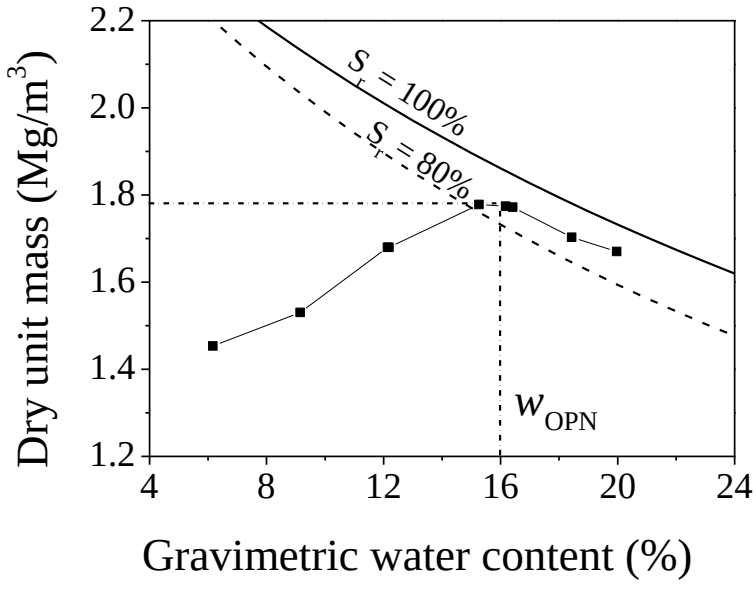

Figure 2: Normal proctor curve of the sub-soil

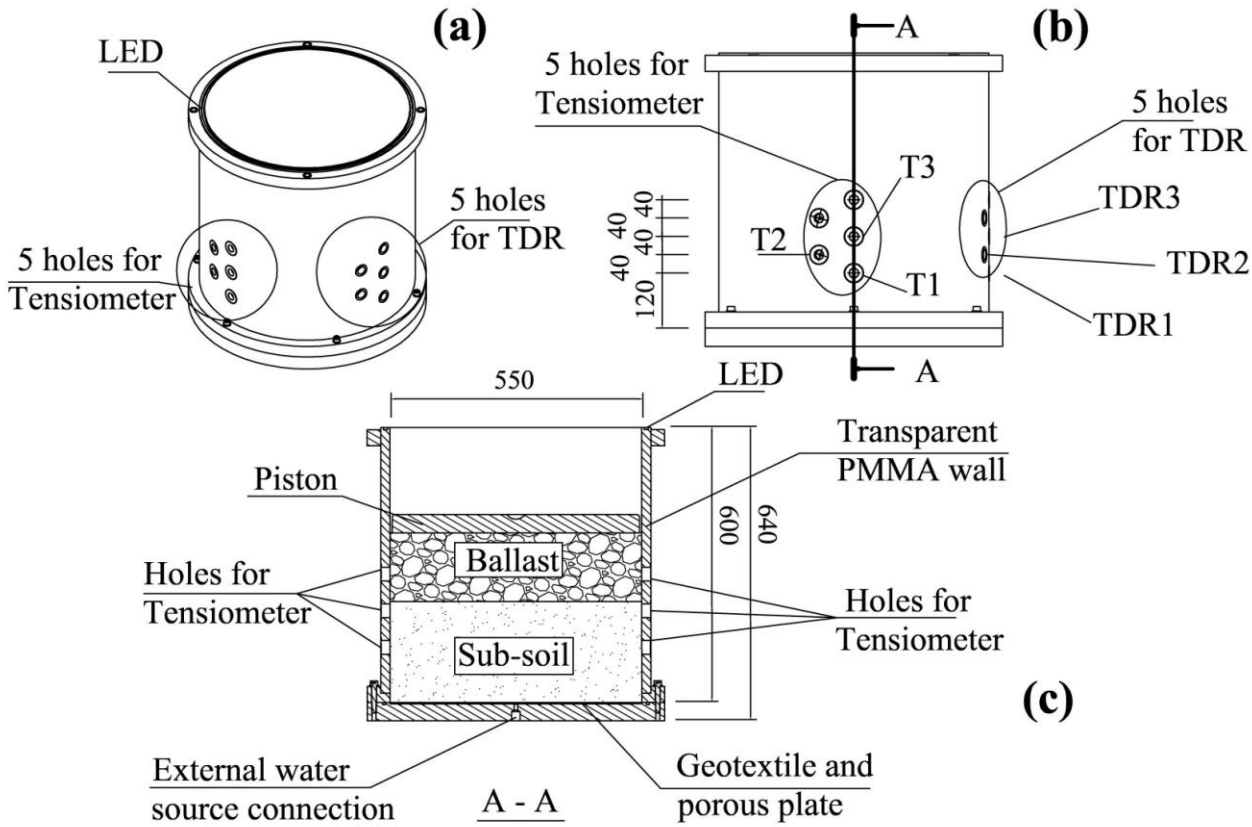

Figure 3: Schematic view of the apparatus

Figure 4: Photograph of the physical model

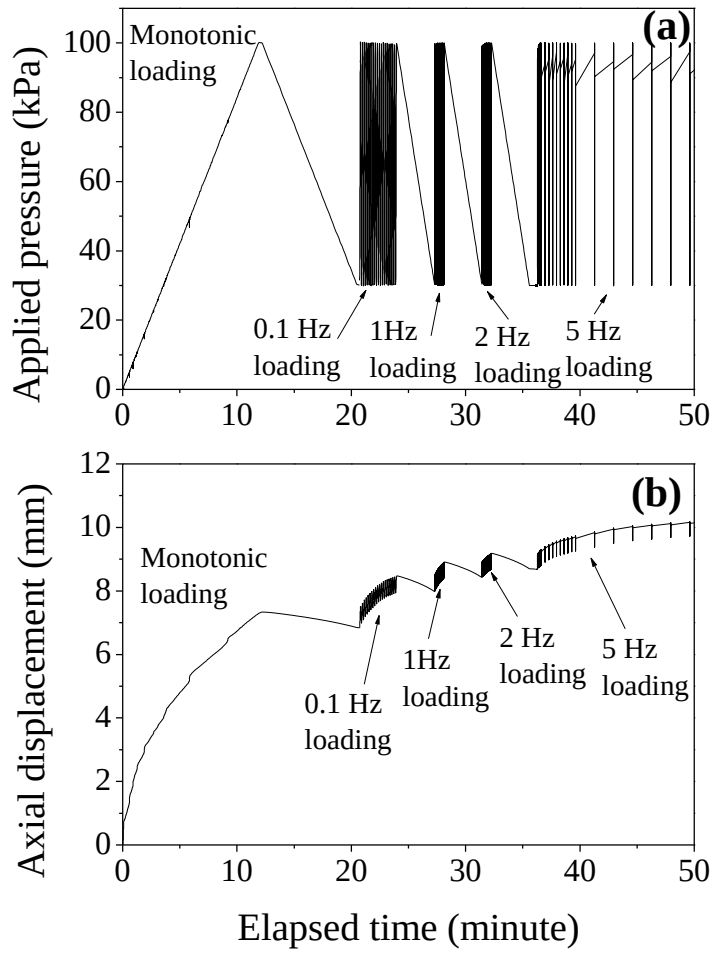

Figure 5: Pre-loading in *Unsaturated state*

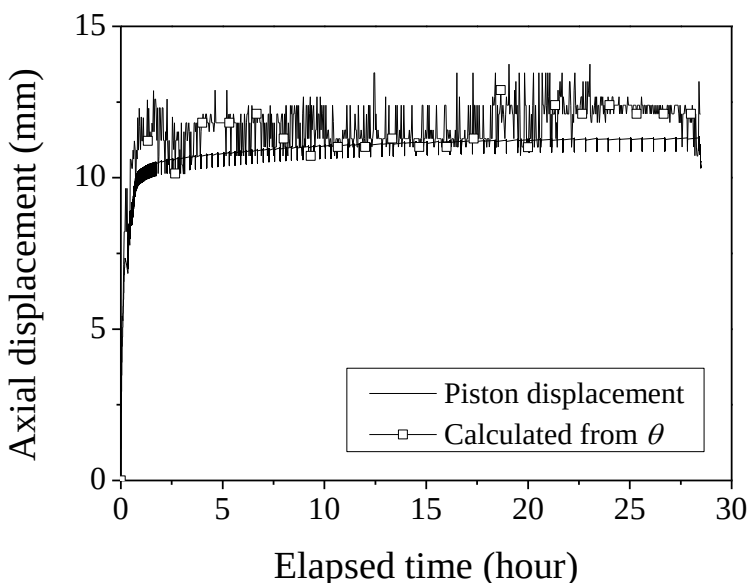

Figure 6: Axial displacement during loading in *Unsaturated state*

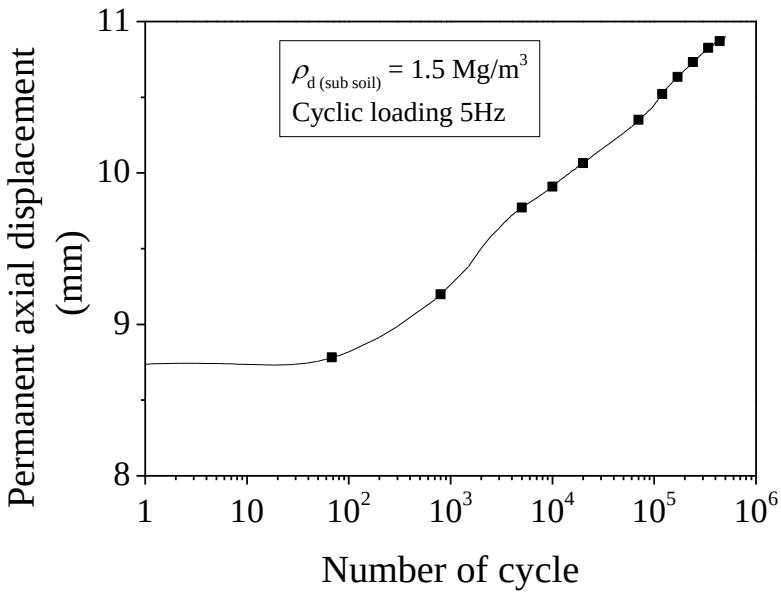

Figure 7: Displacement during cyclic loading at 5 Hz in *Unsaturated state*

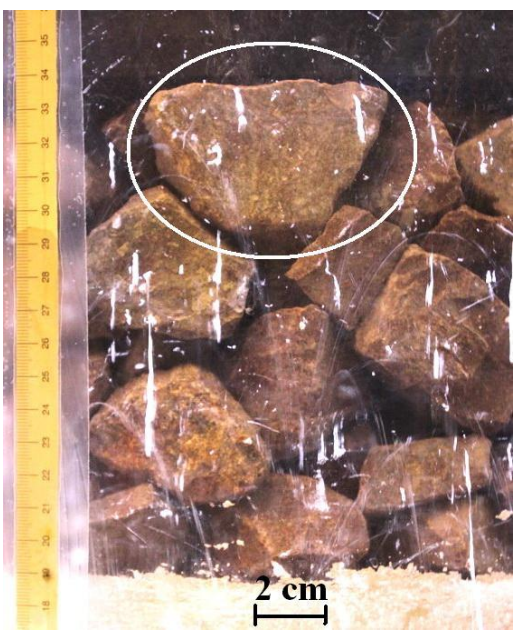

a) Reference ballast particle

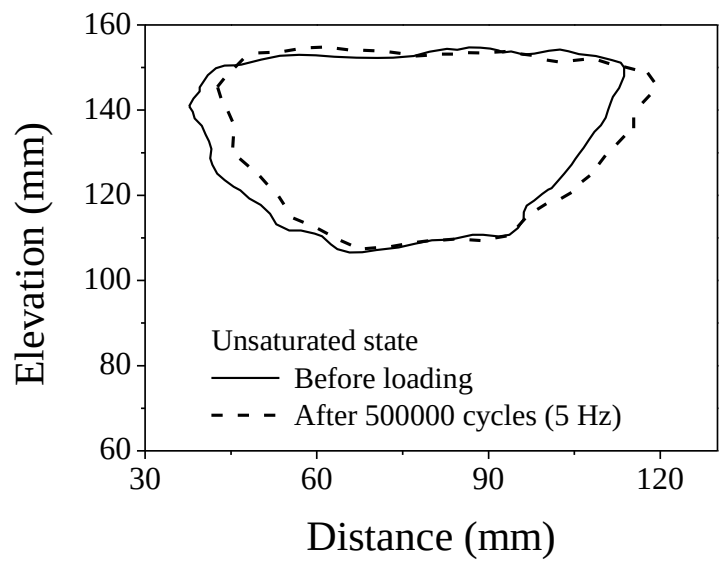

b) Outline ballast change before and after loading in *Unsaturated state*

Figure 8: Monitoring of one ballast particle movement

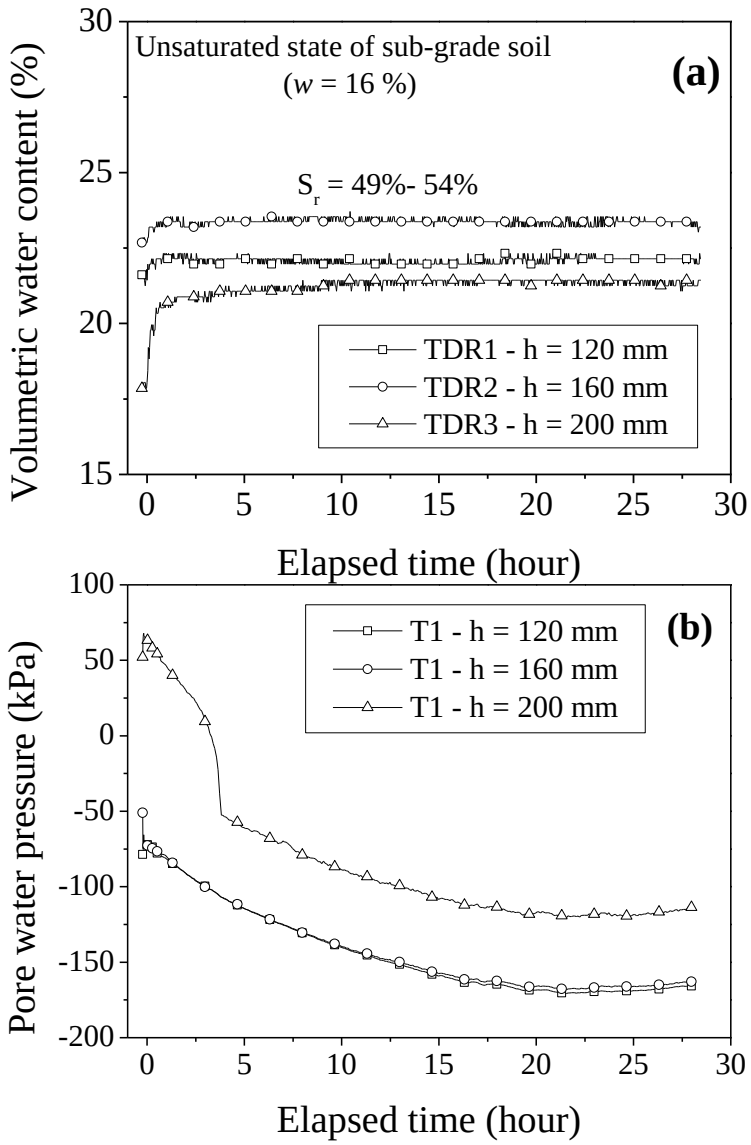

Figure 9: Changes in volumetric water content and pore water pressure in *Unsaturated state*

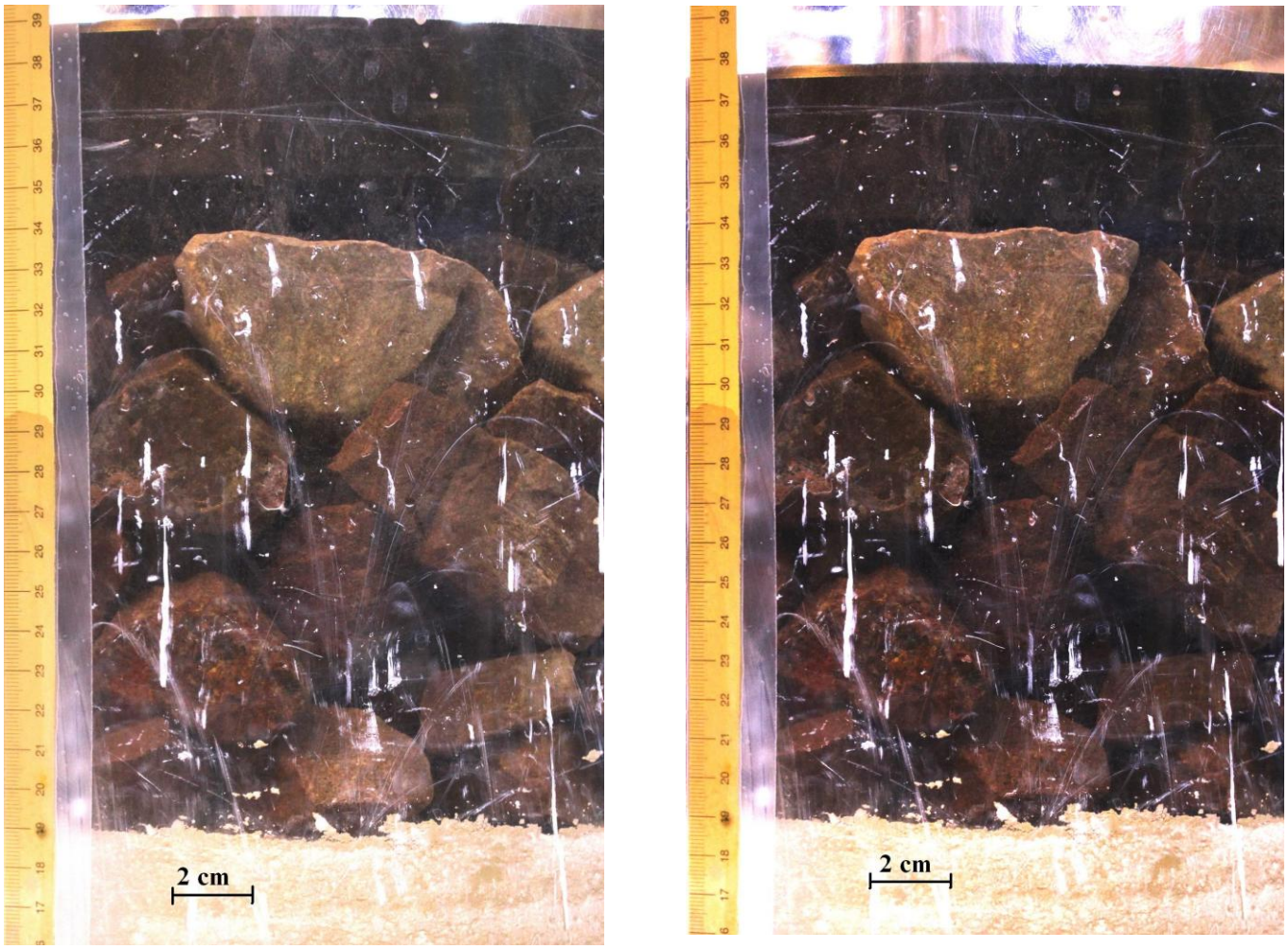

a) Before loading (w = 16%)

b) After loading (w = 16%)

Figure 10: Photographs of the interface between two soils layers: a) before and b) after loading in *Unsaturated state*

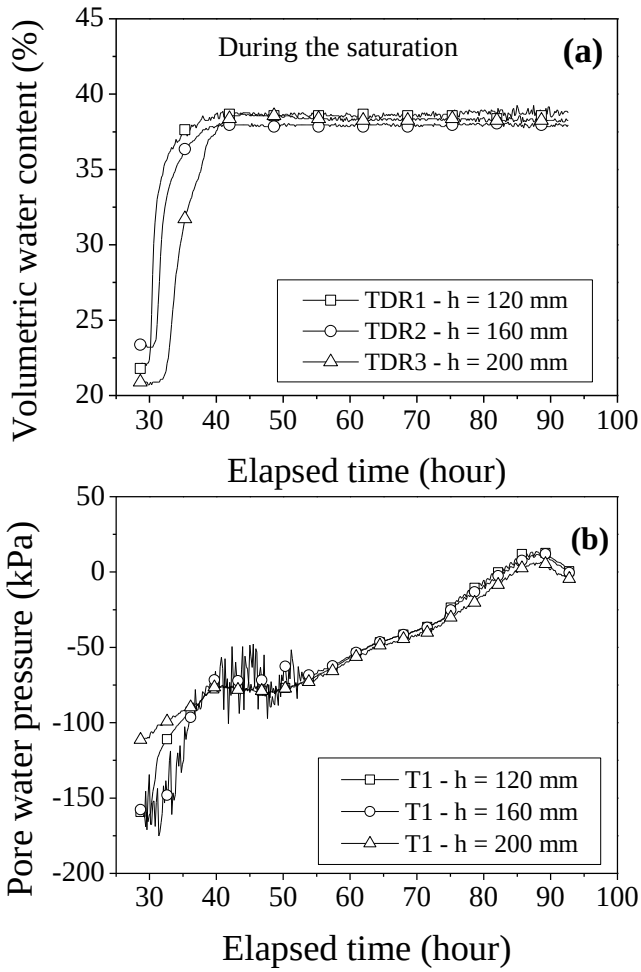

Figure 11: Changes in volumetric water content and pore water pressure during *Saturation*

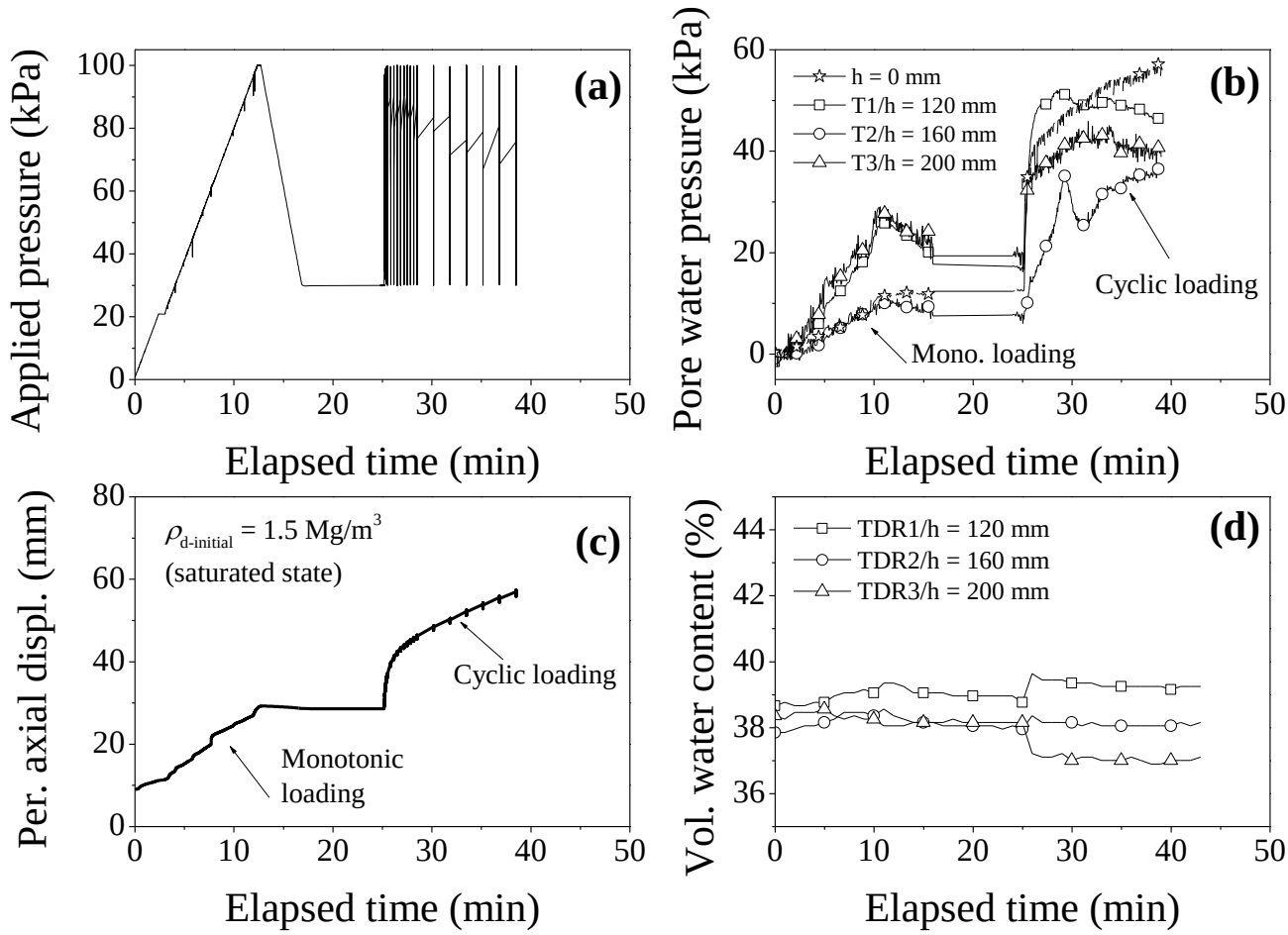

Figure 12: Test on the sub-soil at *Saturated state*: a) applied pressure; b) permanent axial displacement; c) pore water pressure and d) volumetric water content

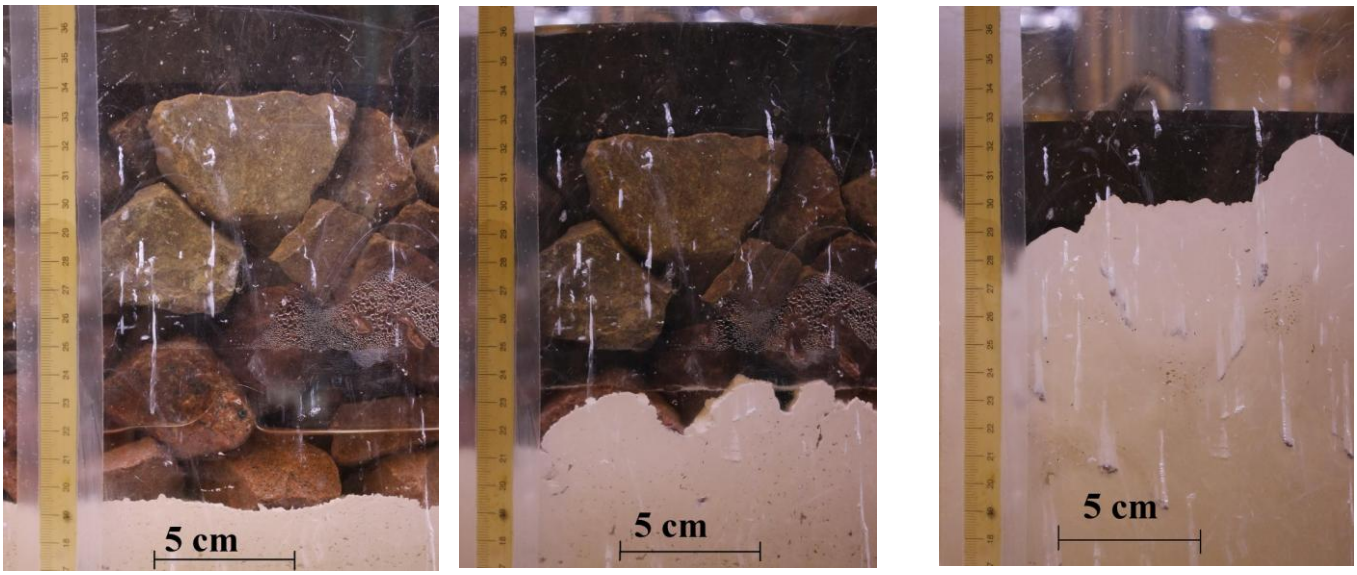

a) after saturation and before monotonic loading

b) after monotonic loading (saturated state)

c) after cyclic loading (saturated state)

Figure 13: Photographs showing the evolution of interface between two the soils layers: fine particles were pumped upwards

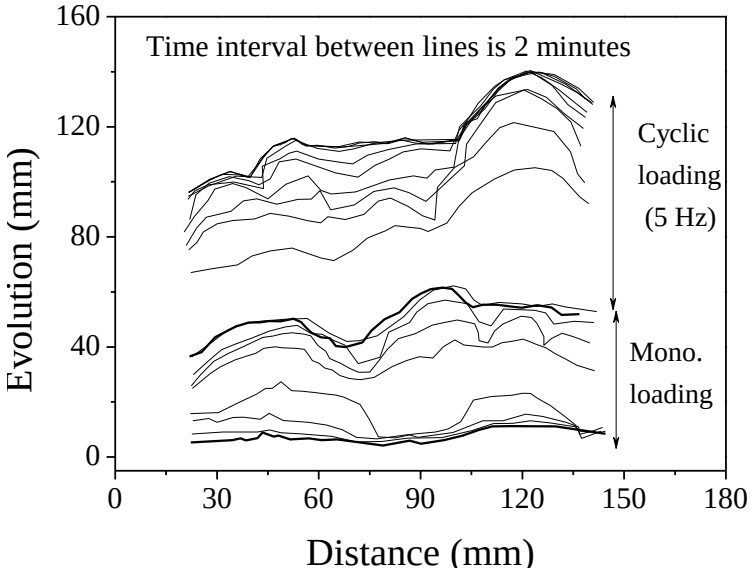

Figure 14: Sub-grade surface evolution

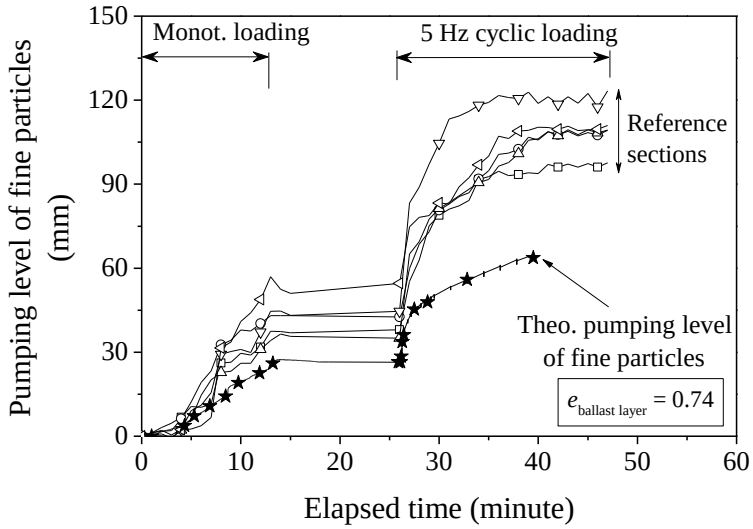

Figure 15: Pumping level of fine particles during the test in *Saturated state*